Microscale Polymer–Nanotube Composites

Erik K. Hobbie,* Jeffrey A. Fagan, Jan Obrzut, and Steven D. Hudson

Polymers Division, National Institute of Standards and Technology, Gaithersburg, Maryland 20899

ABSTRACT Polymer colloids with an interfacial coating of purified single-wall carbon nanotubes (SWCNTs) are synthesized from length- and type-sorted SWCNTs. Aqueous nanotube suspensions sorted through density-gradient ultracentrifugation are used to emulsify spherical polymer colloids of microscale dimensions that are characterized through a combination of optical microscopy, transmission electron microscopy, and impedance spectroscopy. The SWCNT–polymer composite particles exhibit electrical conductivities comparable to or better than those of bulk SWCNT–polymer composites at nanotube loadings of more than 1 order of magnitude lower. The composite particles retain the unique electronic and optical characteristics of the parent SWCNT solution with potential applications as microelectronic and microoptical components.

KEYWORDS: single-wall carbon nanotubes • ultracentrifugation • polymer nanocomposites • emulsions • interfacial assembly • conductivity

INTRODUCTION

The ability to disperse and assemble single-wall carbon nanotubes (SWCNTs) in polymers will be critical to their ultimate commercial success in polymer composites. Although metrics of SWCNT dispersion are well established for polymers (1), a high degree of exfoliation is notoriously difficult to achieve and usually requires a significant amount of surface treatment (2–7) that can ultimately interfere with the ability to impart the desired physical characteristic of the SWCNT to the final polymeric material. To a large extent, this impediment reflects an inherent degree of amphiphobicity that stems from the relatively poor wettability of SWCNTs by most common solvents. A novel consequence of this is the ability of a neat SWCNT material to act as a nanoparticle "surfactant" in the emulsification of immiscible liquids such as water and toluene (8).

Known as Pickering emulsions, particle-stabilized droplets of immiscible fluids have been used for years in industrial processes like oil recovery and wastewater treatment, but they have recently received renewed interest as novel platforms for particle manipulation and interfacial self assembly (9–17). Contemporary applications range from the stabilization of polymer colloids (18, 19) to the preparation and synthesis of metal–oxide microspheres (20) and thermosensitive colloidosomes (21, 22). For the specific scenario in which the stabilizing particle is a carbon nanotube, interfacial trapping between immiscible fluids has recently been demonstrated as a viable route to SWCNT purification (23, 24), the assembly of flexible SWCNT films for enhanced electron transfer (25), the electrochemical synthesis of nanoporous composites of nanotube-doped conducting polymers (26), and the synthesis of porous polymer foams (27). The efficient manner in which neat carbon nanotubes preferentially segregate to immiscible fluid–fluid interfaces immediately opens up new potential routes to polymer nanocomposite processing and assembly by exploiting their poor solubility. Such approaches would bypass undesirable effects associated with the treatment or coating of the nanotube surface, such as a reduction in the electrical conductivity due to inhibited interfacial contact between mechanically percolated nanotubes (28). A macroscopic variation on this theme has recently been used to produce conductive "cellular" carbon nanotube polymer composites that exhibit enhanced conductivity at reduced nanoparticle loadings (29).

Here, we report a process for synthesizing microscopic cross-linked polymer colloids with an interfacial coating of type- or length-purified SWCNTs. Aqueous suspensions of SWNCTs purified and sorted through density-gradient ultracentrifugation in the biological surfactant sodium deoxycholate (DOC) are used to emulsify a methacrylate monomer that is then polymerized into spherical polymer colloids of 1–20 μm diameter. As prepared, these particles are stabilized in water by the combined effect of SWCNT and DOC. The addition of ethanol to the suspension fully solubilizes the DOC, causing neat SWCNT to condense onto the polymer interface. The resulting nanocomposite microspheres are characterized using a combination of optical microscopy, transmission electron microscopy (TEM), and impedance spectroscopy. They retain the unique electronic and optical characteristics of the parent SWCNT solution and can be readily assembled on surfaces for potential applications that require microelectronic components. The purified nature of the SWCNT coating yields material conductivities comparable to those reported by Mu et al. (29) but at SWCNT loadings over 1 order of magnitude lower.

MATERIALS AND METHODS

Dispersion of the different SWCNT powders, NASA-JSC laser ablation batch 338 and SWeNT cobalt–molybdenum catalyst (CoMoCat) SG65-000-0024, was performed as described in

* To whom correspondence should be addressed. E-mail: erik.hobbie@nist.gov.
Received for review March 31, 2009 and accepted June 11, 2009

DOI: 10.1021/am9002205

detail elsewhere (32, 33). Briefly, the SWCNT preparation consisted of sonication (tip sonicator, 0.64 cm) of the SWCNT powder loaded at 1.0 ± 0.1 mg/mL in a 2% by mass sodium deoxycholate (DOC) aqueous surfactant solution for 1.0−1.5 h in 32 mL batches in an ice−water bath at 27−30 W of applied power. After sonication, each suspension was centrifuged for 2 h at 1885 rad/s and 12 °C in a Beckman-Coulter JA-20 rotor (at approximately 39 000*g*) and the supernatant collected.

Electronic-type separated laser SWCNTs were prepared using a method similar to that of Arnold et al. in ref 30 and Yanagi et al. in ref 31. However, for the laser SWCNTs, an additional separation that enriches the SWCNT population after dispersion but before type separation was performed in a Beckman-Coulter VTI 65.2 vertical rotor for 1 h at 6800 rad/s and 20 °C with the following density layers: 1 mL of 18 % mass per volume iodixanol (5,5′-[(2-hydroxy-1,3-propanediyl)bis(acetylamino)]-bis[*N*,*N*′-bis(2,3-dihydroxylpropyl-2,4,6-triiodo-1,3-benzenecarboxamide)]), 1% DOC; 3 mL of 9% mass per volume iodixanol, 1% DOC; 0.9 mL of 2% DOC, SWCNTs. A consistent middle band was collected and multiple runs were concentrated via forced filtration (32) to produce the parent dispersion for type separation. This fractionation improves the yield of the electronic-type separation and appears to narrow the chirality distribution of the sample. Electronic-type separation was performed in a Beckman-Coulter SW-32 rotor for 19.25 h at 3350 rad/s and 20 °C. The solution layers for electronic separation were as follows: 1 mL of 40% mass per volume iodixanol, 0.75% sodium dodecylsulfate (SDS), 0.75% sodium cholate (NaChol); 2 mL of purified SWCNTs in 32% iodixanol, 1.125% SDS, 0.5% DOC; 20 mL of 30% mass per volume iodixanol, 1.125% SDS, and 1.125% NaChol. The laser SWCNT dispersion used in the separation was allowed to equilibrate in the mixed-surfactant environment for at least 4 days prior to separation. After separation, metallic and semiconducting fractions were collected and dialyzed repeatedly via forced filtration against a 30 kD membrane to exchange the SWCNTs into 1% DOC and to increase the absolute SWCNT concentration.

Length-sorted CoMoCat SWCNTs were also produced using ultracentrifugation (32). The original aqueous stock solution of 2% by mass DOC was density modified for length separation by mixing the appropriate surfactant and SWCNT solution with iodixanol and 2% by mass DOC (32). A Beckman-Coulter L80-XP ultracentrifuge with a swinging-bucket Ti rotor was used with the SW-32 bucket sets for the length separation. The prepared (layered) centrifuge tube contained 24 mL of liquid in four layers: 1 mL of 35% iodixanol, 1 mL of 30% iodixanol, 2 mL of 20% iodixanol containing SWCNTs, and 20 mL of 15% iodixanol in the top layer. All layers contained 2% DOC. Separation was performed at 2649 rad/s for 21 h at 4 °C. After separation, individual fractions were collected by pipetting in 0.75 mL increments. A broad long fraction was extracted for this work, and the mean SWCNT length ($L \approx 900$ nm) was established empirically using optical spectroscopy (32, 33). A consistent measure of the SWCNT concentration is obtained from the ratio of the absorbance at 775 nm (CoMoCat) or 800 nm (NASA laser SWCNTs) in the sonicated, precentrifuged SWCNT suspension (for which the SWCNT mass fraction is precisely known) to the corresponding absorbance for the final fraction as a measure of the SWCNT mass loss. These wavelengths were chosen because they lie away from the optical resonance features and are thus less sensitive to any length-dependent optical effects (32, 33).

Cross-linked polymer colloids were synthesized from 1:1 volume mixtures of a 1,12-dodecanediol dimethacrylate (C_{12}DMA) monomer with a 1% benzoyl peroxide initiator and C_{12}DMA with a 0.5% *N*,*N*-dimethyl-*p*-toluidine accelerator and a 0.1% ferrocene catalyst. These components were premixed, and the resulting organic liquid was mechanically emulsified in the SWCNT−DOC suspension at a nominal ratio of 2:1 aqueous to organic. Pure aqueous DOC solutions were ineffective emulsifiers, suggesting that detached DOC and SWCNT act in tandem to stabilize emulsions of the liquid monomer, as shown schematically in Figure 1. Control (SWCNT-free) colloids were thus emulsified in a 2% SDS solution. To condense the SWCNT fully onto the cross-linked polymer interface, the multiphase aqueous colloidal suspensions were subsequently diluted and vigorously mixed 10:1 with ethanol, which is a good solvent for DOC. The SWCNT-coated polymer colloids were then lightly centrifuged or allowed to gravitationally settle before washing repeatedly with ethanol to remove DOC, leaving SWCNT-dressed polymer colloids in ethanol (Figure 1c).

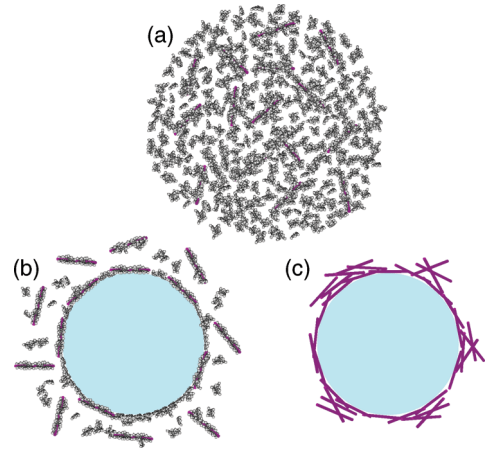

FIGURE 1. (a) Initial aqueous SWCNT suspension containing both surfactant-coated SWCNT and free DOC above the critical micelle concentration of the surfactant. (b) In this aqueous environment, the liquid monomer (light blue) forms an emulsion stabilized by both the surfactant and the SWCNT. (c) After polymerization of the monomer, rinsing of the colloidal suspension in ethanol removes the DOC and condenses the SWCNT interphase onto the cross-linked polymer colloid.

Single- and double-stranded DNA have also been shown to be effective dispersants for SWCNTs in aqueous environments (1, 34−36). By variation of the pH or ionic strength of the suspension, analogous polymer colloids have been synthesized (37) that are coated and stabilized in water by a robust interfacial layer of ssDNA-wrapped nanotubes. Because of the nearly permanent absorption of ssDNA onto SWCNT, these particles retain a robust hydrophilic coating despite a lack of free ssDNA in the initial SWCNT solutions. For comparison, nanotube-coated dimethacrylate colloids were thus also synthesized with ssDNA-wrapped SWCNTs. Stock suspensions of SWCNT in ssDNA were prepared by sonication in an ice−water bath (10 W, 3.2 mm tip sonicator) of 1 mg/mL nanotubes in a salt solution (0.2 mol/L NaCl, 0.04 mol/L Tris, HCl to pH = 7.0) in the presence of 1 mg/mL 30-mer 5′-GT$(GT)_{13}$GT-3′ single-stranded DNA (Integrated DNA Technologies) for 2 h, followed by centrifugation (2 h at 21 000*g*). The resulting supernatant has been previously shown to contain well-dispersed individual nanotubes (1).

UV−vis−near-IR (NIR) absorption spectroscopy was performed in transmission mode on a PerkinElmer Lambda 950 UV−vis−NIR spectrophotometer over the wavelength interval 2500−185 nm. The incident light was depolarized prior to the sample compartment, and the measurement was corrected for the dark current and background spectra; data were recorded at 1 nm increments with an instrument integration time of 0.16 s per increment. Additionally, the reference beam was left unobstructed, and the subtraction of the appropriate reference sample was performed during data reduction. Where applicable, fluorescence maps for stock SWCNT solutions were generated using a JY-Horiba Fluorolog-3 spectrofluorometer. Data were corrected for the instrument's source spectral dis-

tribution, detector/grating spectral response, and absorbance of the long-pass filter used to restrict scattered excitation light from the NIR detector. The excitation wavelength was scanned in 5 nm increments using a 450 W xenon lamp through a 6 nm slit and a 1200 lines/mm monochromator with a 500 blaze. The emission passed through a long-pass filter and was measured on a liquid-nitrogen-cooled InGaAs array in 1.6 nm increments through a 6 nm slit and a 100 lines/mm monochromator with an 800 blaze.

Bright-field, phase-contrast, and fluorescence optical microscopy were performed on an Olympus 1X71 inverted microscope. NIR fluorescence capability (38, 39) in epi-illumination was achieved using an Olympus 60× UPlanApo 1.2 NA water-immersion or Nikon 20× CF Plan EPI ELWD objective, a liquid-nitrogen-cooled InGaAs CCD, and band-pass optics dictated by the absorption and emission spectra of the parent SWCNT suspension. Bright-field and phase-contrast images were collected simultaneously in transmission with the same objective on the same microscope. Reflectance microscopy of the colloids assembled on micropatterned circuits was performed with a Nikon Labophot-2 with 5× and 10× E Plan BD objectives. Image analysis was done with ImageJ. For TEM measurements, polymerized particles were dried and then cast in a matrix of either the identical dimethacrylate resin or an epoxy formulation (Araldite, Embed 812, from Electron Microscopy Sciences). The embedded composites were then cured at 55 °C overnight, and the resulting block was trimmed and microtomed at room temperature using an ultrasonically vibrating diamond knife (Diatome and Leica Ultracut). Sections of approximately 70 nm in thickness were retrieved on copper grids for bright-field observation with a Philips EM400T, operated at 120 kV, with a slight underfocus.

For impedance spectroscopy measurements, a test structure of varied electrode spacing (5−20 μm) was patterned on a highly doped silicon substrate with a dielectric silicon oxide layer of 200 nm thickness using photolithography. A gold film was evaporated on the bottom surface for application of a gate voltage. Contacts to the test structure were made using 4T coaxial probes on a Cascade Probe Station. Measurements of the complex impedance were conducted in the frequency range 40 Hz $< f <$ 1 MHz through a four-terminal technique using the Agilent 4294A Precision Impedance Analyzer, calibrated to a 50 Ω load standard from Cascade. Colloids were assembled on the electrodes by micropipetting the desired volume of the ethanol suspension into a larger plastic pipette tip fixed over the targeted coordinates of the test structure. After the ethanol evaporated, the wafer was annealed in a vacuum oven at 100 °C and the specific arrangement of contacted colloids spanning the electrodes at each test site was measured by reflectance microscopy. Impedance was converted to resistivity using the optically measured spacing between electrodes and the optically measured arrangement of contacted polymer particles between electrodes.

RESULTS AND DISCUSSION

The electronic and optical properties of SWCNTs are dictated by their electronic band structure, which is specified by the chiral vector (n, m) characterizing the symmetry of rolling a 2D graphene sheet into a hollow tube of diameter a. The semiconducting SWCNTs have a band gap defined by cusplike singularities in the electronic density of states arranged symmetrically on either side of the Fermi level (40), denoted as *11*, *22*, *33*, etc., in order of increasing energy. In isolation, the optical absorption spectra of such SWCNTs show sharp peaks associated with electronic interband transitions (40−42). Laser SWCNTs are relatively large diameter nanotubes and consequently contain a continuum

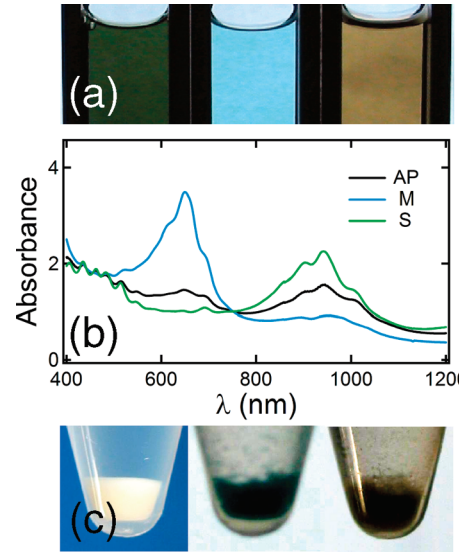

FIGURE 2. (a) Laser SWCNTs after the initial coarse purification (left, 35 μg/mL SWCNT, AP), the final blue metallic (M) fraction (middle, 60 μg/mL SWCNT) and the final brown-yellow semiconducting (S) fraction (right, 110 μg/mL SWCNT). (b) UV−vis−NIR absorption spectra of the three suspensions in part a. (c) Sedimented polymer colloids in ethanol from the SDS-synthesized control (left), polymer colloids coated with blue metallic SWCNTs (middle), and colloids coated with semiconducting SWCNTs (right).

of chiralities. Figure 2a shows the different-colored SWCNT solutions from the type sorting of the laser SWCNTs with the corresponding UV−vis−NIR absorption spectra in Figure 2b. The final concentrations of the metallic and semiconducting fractions are 60 and 110 μg/mL, respectively. The prominent absorption peak in the red for the metallic suspension (M) corresponds to the first (*11*) metallic interband transition and renders the solution bright blue. The prominent peak in the NIR for the semiconducting fraction corresponds to the second (*22*) semiconducting interband transition, and the broad background absorption in the visible makes this fraction brownish yellow in appearance. These colors are preserved in the SWCNT-coated colloids (Figure 2c), which for comparison appear white when synthesized with SDS (Figure 2c, left).

Figure 3a shows the UV−vis−NIR absorption spectrum from a dilution of the length-purified CoMoCat SWCNT suspension. This material has a natural enrichment in the (6,5) and (7,5) semiconducting species, respectively, and a particularly intriguing consequence of the band structure of these nanotubes is a fluorescent emission triggered by the absorption of a photon across the *22* transition and the subsequent reemission across the *11* transition. Figure 3b shows a plot of this photoluminescence (PL) as measured in the plane of excitation and emission wavelengths. The dominant absorption peak at around 980 nm in Figure 3a corresponds to the *11* transition of the (6,5) SWCNT, with a corresponding bright PL feature in the NIR (Figure 3b). The 27 μg/mL SWCNT fraction is dark purple to black in color and forms diffuse nonsedimenting SWCNT flocs upon dilution in ethanol, as shown in the top panel of Figure 3c. In contrast, the SWCNT-coated polymer microspheres slowly sediment out of ethanol (bottom panel, Figure 3c) but can be easily redispersed by shaking.

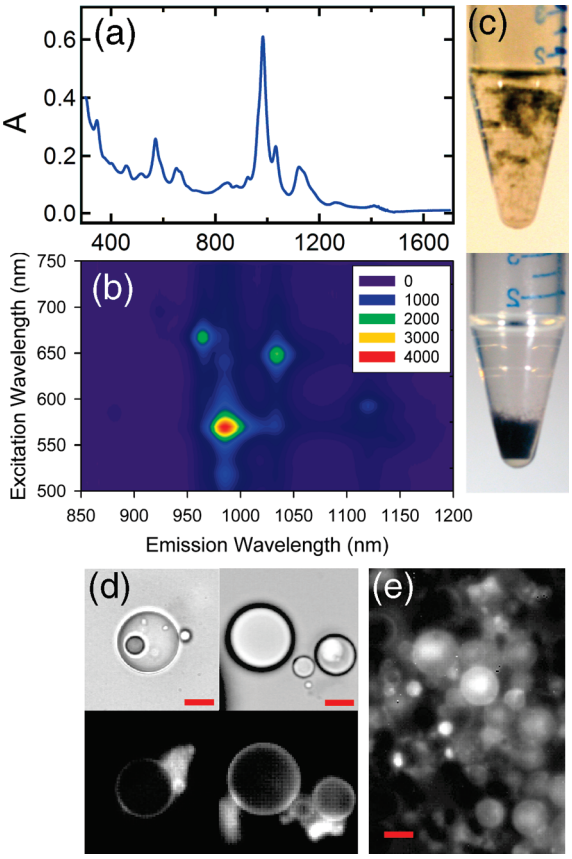

FIGURE 3. (a) UV−vis−NIR absorption spectrum as a function the (nm) for the length-enriched CoMoCat SWCNT suspension. (b) PL plot of the same fraction in the plane of excitation wavelength versus emission wavelength. (c) Neat surfactant-free SWCNTs (top) and SWCNT-coated colloids (prepared from the length-purified CoMoCat SWCNTs at 27 μg/mL) in ethanol after the same time period (1 h). (d) Bright-field (top) and NIR-fluorescence (bottom) optical micrographs of the CoMoCat SWCNT-coated colloids synthesized as described in this paper (left) and using comparable nanotubes coated with single-stranded DNA (right). The scale bar in each image is 10 μm. (e) NIR-fluorescent micrograph of dried CoMoCat SWCNT-coated colloids (scale bar = 20 μm).

Figure 3d shows a comparison of bright-field (top) and NIR-fluorescent (bottom) micrographs for the neat CoMoCat-coated colloids (left) and colloids synthesized using comparable SWCNTs wrapped with ssDNA (right), where the scale bar in each image is 10 μm. Both interfacial layers exhibit a luminescent corona around the colloid interface. In contrast, control colloids synthesized with SDS exhibited no PL. Note that bright field is measured in transmission while NIR fluorescence is measured in epi-illumination and stacked colloids evident in the bright field are thus not visible in fluorescence. Figure 3e shows an NIR-fluorescent image of the CoMoCat-coated colloids after repeated rinsing in ethanol and subsequent drying in a vacuum oven.

Typical impedance spectroscopy data are shown in Figure 4a. Control colloids synthesized with SDS and rinsed repeatedly in ethanol showed purely dielectric behavior with no measurable conductivity. In contrast, data for both the metallic and semiconducting spheres show a low-frequency plateau in the real part of the response with imaginary parts that asymptote to the response of the SWCNT-free control. A reflectance micrograph of a typical bridge is shown in

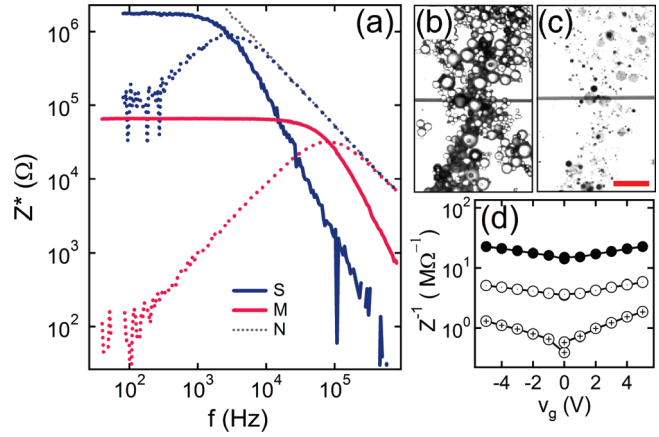

FIGURE 4. (a) Real (solid) and imaginary (dashed) part of impedance versus frequency for the blue metallic-coated colloids (M), the yellow-brown semiconducting-coated colloids (S), and the white control colloids (N) shown in Figure 2. No real (conductive) part was measurable for the control, while the imaginary (capacitive) part of M and S both asymptote to the control at high frequency. All samples correspond to the same fractional coverage of a 10 μm gap between micropatterned gold electrodes on silicon. (b) Reflectance optical micrograph of a percolated path for sample M and (c) the same region after impregnating the assembly with the cross-linked polymer resin (scale bar = 100 μm). (d) Inverse impedance at 500 Hz as a function of the gate voltage for the metallic-laser (solid circles), CoMoCat length-sorted (open circles with dots), and semiconducting-laser coated (open circles with crosses) colloids.

Figure 4b, where the scale bar is 100 μm. The white background corresponds to gold electrodes, with the 10 μm gap apparent as a thin horizontal dark band in the middle of the image. Filling the assembly with the neat polymer resin (Figure 4c) reveals the SWCNT shells of the percolated polymer spheres.

The inverse impedance at 500 Hz as a function of the gate voltage V_g for typical assemblies printed with metallic, CoMoCat, and semiconducting spheres is shown in Figure 4d. The metallic NASA−JSC composite spheres (M) show the highest conductivity, followed by the length-purified CoMoCat (which contains a nominal metallic content (43) of 15%) and the semiconducting NASA−JSC (S). The ambipolar nature of the response is most pronounced for the semiconducting-coated spheres and is typical of what is measured for SWCNT-network devices (44). It is somewhat suppressed here because of the doubly percolated nature of the spherical contacts across the electrodes. At a gate voltage of 5 V, based on a common 40% coverage of a 10 μm gap to a mean height of 20 μm, we extract a material resistivity of 400 Ω m for S (SWCNT fraction of 2.2×10^{-4} g/mL), 40 Ω m for M (SWCNT fraction of 1.2×10^{-4} g/mL), and 100 Ω m for length-enriched CoMoCat (SWCNT fraction of 5×10^{-5} g/mL). The metallic-coated polymer colloids give 40 Ω m at a SWCNT loading of 0.012%, which is a factor of 25 below the estimated bulk percolation threshold quoted in ref 45. Just above bulk percolation, ref 45 reports a resistivity of 100 Ω m at a SWCNT volume fraction of 0.6%, while the cellular polymer composites in ref 29 have 33 Ω m at 0.5% SWCNT. Printing the same batch of metallic-coated colloids on different electrodes of the same test pattern gave 10 Ω m at 45% gap coverage, 40 Ω m at 40% gap coverage, and 100 Ω m at 6% gap coverage. The

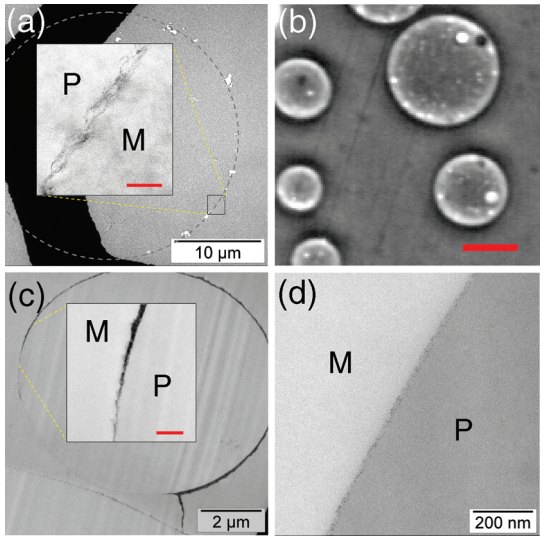

FIGURE 5. (a) TEM image of a microtomed slice of the composite obtained when the matrix (M) and particle (P) are both cross-linked dimethacrylate (inset scale bar = 200 nm). (b) Encasing the particles in epoxy gives sufficient contrast to resolve the particle and matrix through phase-contrast optical microscopy of the slice (scale bar = 20 μm). (c) TEM on epoxy matrix slices showing the interface decorated with an amorphous SWCNT network (scale bar = 200 nm), which varies in thickness. (d) High-resolution image of a region of thin SWCNT interface. All particles are synthesized from 35 μg/mL laser SWCNT suspensions.

systematic decrease in resistivity with increasing coverage suggests that the number of percolation pathways increases strongly with the number of contacted spheres at these length scales. We obtain the quoted resistivity from the measured impedance and the known separation of electrodes using the optically measured average cross-sectional area of the total bridge for each test site. This treats the material spanning the electrodes as a continuum rather than a percolated assembly of spheres, implying that these values represent upper bounds to the bulk resisitivity.

The process we describe yields conductivities that are comparable to the best low-particle loading protocols that have been achieved to date but at SWCNT volume fractions that are up to 40 times lower. The superior performance stems from the doubly percolated microcellular structure and the ultrapure nature of the SWCNT coating layer. Figure 5a shows TEM images of microtomed polymer composites prepared with identical particle (P) and matrix (M) resins from NASA–JSC laser SWCNT suspensions prepared at 35 μg/mL SWCNT. The interfacial coating of percolated SWCNTs can be seen in the inset. Using epoxy as the matrix adds additional contrast between the particles and the continuous phase, as shown in Figure 5b,c. The SWCNT coating varies from a nominal thickness of 10 to 100 nm, with fibrous strands occasionally extending out into the matrix to length scales of over 1 μm (Figure 5c). The metallic-enriched SWCNT coating imparts the highest electrical conductivity to the percolated assembly of coated microspheres. A simple calculation relates the SWCNT volume fraction of the composite (c) to that of the conducting shell (ϕ); $c = 4\pi R^2 w/(4/3)\pi R^3$, where R is the radius of the polymer particle and w is the thickness of the SWCNT shell. Using the typical measured values $R = 10$ μm and $w = 100$ nm, $c = 0.012\%$ implies $\phi \approx 0.4\%$, comparable to the SWCNT volume fraction cited above from ref 45. Although increasing the nanotube length can improve the conductivity by lowering the percolation threshold, our results suggest that controlling the type is more critical.

CONCLUSIONS

We have synthesized microscopic polymer colloids with an interfacial coating of purified SWCNTs. SWCNTs dispersed in water using the relatively inexpensive surfactant sodium DOC have been sorted through density-gradient ultracentrifugation by both type and length and used to emulsify spherical polymer colloids of microscale dimensions. Characterization of these composite particles through a combination of optical microscopy, TEM, and impedance spectroscopy reveals a thin shell or "interphase" of pure carbon nanotubes around a pure polymer core. The SWCNT–polymer nanocomposite particles exhibit electrical conductivities comparable to those of previously engineered SWCNT–polymer composites but at nanotube loadings that are more than 1 order of magnitude smaller, a consequence of the microcellular morphology of the assembled polymer particles and the enhanced metallic content in the interfacial SWCNT coating. Of the three materials considered, the SWCNT coating enriched in semiconducting nanotubes yields the lowest electrical conductivity because of the removal of a significant fraction of metallic SWCNTs. The length-purified CoMoCat material is intermediate in conductivity. Although this may be due, in part, to increased percolation anticipated for longer SWCNTs, we suggest that the nominal metallic content of the CoMoCat materials is the dominant reason for this trend.

We conclude by noting two other recent studies that use somewhat similar approaches to produce conducting interfacial assemblies of carbon nanotubes. Matsui and co-authors (46) have engineered thin conducting SWCNT films by exploiting the solubility of SDS in ethanol. Their process creates planar surfactant-free SWCNT films at liquid–liquid interfaces that exhibit excellent transparency and superior conductivity. Hermant and co-authors (47) have exploited the immiscibility of oil–water mixtures to engineer conductive polymer foams with remarkably low SWCNT loadings, also using SDS to exfoliate SWCNTs in an initial aqueous phase. These same authors have recently demonstrated, however, that poly(3,4-ethylenedioxythiophene)–poly(styrenesulfonate) can be substituted for SDS to further reduce the percolation threshold of conducting SWCNT–polymer composites (48). On the basis of our results, we anticipate that these approaches would be significantly improved upon by enrichment of the metallic content of the starting SWCNT suspensions.

REFERENCES AND NOTES

(1) For example, see: Fagan, J. A.; Landi, B. J.; Mandelbaum, I.; Simpson, J. R.; Bajpai, V.; Bauer, B. J.; Migler, K.; Hight Walker, A. R.; Raffaelle, R.; Hobbie, E. K. *J. Phys. Chem. B* **2006**, *110*, 23801, and references cited therein.

(2) Wang, H.; Zhou, W.; Ho, D. L.; Winey, K. I.; Fischer, J. E.; Glinka, C. J.; Hobbie, E. K. *Nano Lett.* **2004**, *4*, 1789.

(3) Schaefer, D. W.; Justice, R. S. *Macromolecules* **2007**, *40*, 8501.
(4) Vaisman, L.; Wagner, H. D.; Marom, G. *Adv. Colloid Interface Sci.* **2006**, *128*, 37.
(5) Vaisman, L.; Wachtel, E.; Wagner, H. D.; Marom, G. *Polymer* **2007**, *48*, 6843.
(6) Ham, H. T.; Choi, Y. S.; Chung, I. J. *J. Colloid Interface Sci.* **2005**, *286*, 216.
(7) Douroumis, D.; Fatouros, D. G.; Bouropoulos, N.; Papagelis, K.; Tasis, D. *Int. J. Nanomed.* **2007**, *2*, 761.
(8) Wang, H.; Hobbie, E. K. *Langmuir* **2003**, *19*, 3091.
(9) He, Y. J.; Qi, S. T.; Zhao, S. Y. *Prog. Chem.* **2007**, *19*, 1443.
(10) Huang, W. A.; Lan, Q.; Zhang, Y. *Prog. Chem.* **2007**, *19*, 214.
(11) Zeng, C.; Bissig, H.; Dinsmore, A. D. *Solid State Commun.* **2006**, *139*, 547.
(12) Lin, Y.; Boke, A.; Skaff, H.; Cookson, D.; Dinsmore, A. D.; Emrick, T.; Russell, T. P. *Langmuir* **2005**, *21*, 191.
(13) Tarimala, S.; Ranabothu, S. R.; Vernetti, J. P.; Dai, L. L. *Langmuir* **2004**, *20*, 5171.
(14) Tarimala, S.; Dai, L. L. *Langmuir* **2004**, *20*, 3492.
(15) Chen, K.; Yang, Y.; Sa, Q.; Shi, L.; Zhao, H. *Polymer* **2008**, *49*, 2650.
(16) Liu, Y. Y.; Chen, X. Q.; Wang, R. H.; Xin, J. H. *Mater. Lett.* **2006**, *60*, 3731.
(17) He, Y. J. *Mater. Lett.* **2005**, *59*, 114.
(18) Lawrence, D. B.; Cai, T.; Hu, Z.; Marquez, M.; Dinsmore, A. D. *Langmuir* **2007**, *23*, 395.
(19) Tsuji, S.; Kawaguchi, H. *Langmuir* **2008**, *24*, 3300.
(20) Andresen, M.; Stenius, P. *J. Dispersion Sci. Technol.* **2007**, *28*, 837.
(21) Edmond, K. V.; Schofield, A. B.; Marquez, M.; Rothstein, J. P.; Dinsmore, A. D. *Langmuir* **2006**, *22*, 9052.
(22) Rozenberg, B. A.; Tenne, R. *Prog. Polym. Sci.* **2008**, *33*, 40.
(23) Wang, R. K.; Park, H. O.; Chen, W. C.; Silvera-Batista, C.; Reeves, R. D.; Butler, J. E.; Ziegler, K. J. *J. Am. Chem. Soc.* **2008**, *130*, 14721.
(24) Wang, R. K.; Reeves, R. D.; Ziegler, K. J. *J. Am. Chem. Soc.* **2007**, *129*, 15124.
(25) Zhang, Y. J.; Shen, Y. F.; Kuehner, D.; Wu, S.; Su, Z. M.; Ye, S.; Niu, L. *Chem. Commun.* **2008**, *36*, 4273.
(26) Peng, C.; Snook, G. A.; Fray, D. J.; Shaffer, M. S. P.; Chen, G. Z. *Chem. Commun.* **2006**, *44*, 4629.
(27) Menner, A.; Verdejo, R.; Shaffer, M.; Bismarck, A. *Langmuir* **2007**, *23*, 2398.
(28) Hobbie, E. K.; Obrzut, J.; Kharchenko, S. B.; Grulke, E. A. *J. Chem. Phys.* **2006**, *125*, 044712.
(29) Mu, M. F.; Walker, A. M.; Torkelson, J. M.; Winey, K. I. *Polymer* **2008**, *49*, 1332.
(30) Arnold, M. S.; Green, A. A.; Hulvat, J. F.; Stupp, S. I.; Hersam, M. C. *Nat. Nanotechnol.* **2006**, *1*, 60.
(31) Yanagi, K.; Miyata, Y.; Kataura, H. *Appl. Phys. Express* **2008**, *1*, 034003.
(32) Fagan, J. A.; Becker, M. L.; Chun, J.; Nie, P.; Bauer, B. J.; Simpson, J. R.; Hight Walker, A. R.; Hobbie, E. K. *Langmuir* **2008**, *24*, 13880.
(33) Fagan, J. A.; Simpson, J. R.; Bauer, B. J.; Lacerda, S.; Becker, M. L.; Chun, J.; Migler, K. B.; Hight Walker, A. R.; Hobbie, E. K. *J. Am. Chem. Soc.* **2007**, *129*, 10607.
(34) (a) Zheng, M.; Jagota, A.; Semke, E. D.; Diner, B. A.; McLean, R. S.; Lustig, S. R.; Richardson, R. E.; Tassi, N. G. *Nat. Mater.* **2003**, *2*, 338. (b) Xu, Y.; Pehrsson, P. E.; Chen, L. W.; Ru, Z.; Zhao, W. *J. Phys. Chem. C* **2007**, *111*, 8638.
(35) Cathcart, H.; Nicolosi, V.; Hughes, J. M.; Blau, W. J.; Kelly, J. M.; Quinn, S. J.; Coleman, J. N. *J. Am. Chem. Soc.* **2008**, *130*, 12734.
(36) Enyashin, A. N.; Gemming, S.; Seifert, G. *Nanotechnology* **2007**, *18*, 245702.
(37) Hobbie, E. K.; Bauer, B. J.; Stephens, J.; Becker, M. L.; McGuiggan, P.; Hudson, S. D.; Wang, H. *Langmuir* **2005**, *21*, 10284.
(38) Tsyboulski, D. A.; Bachilo, S. M.; Weisman, R. B. *Nano Lett.* **2005**, *5*, 975.
(39) Tsyboulski, D. A.; Bachilo, S. M.; Kolomeisky, A. B.; Weisman, R. B. *ACS Nano* **2008**, *2*, 1770.
(40) Wang, F.; Dukovic, G.; Brus, L. E.; Heinz, T. F. *Science* **2005**, *308*, 841.
(41) O'Connell, M. J.; Bachilo, S. M.; Huffman, C. B.; Moore, V. C.; Strano, M. S.; Haroz, E. H.; Rialon, K. L.; Boul, P. J.; Noon, W. H.; Kittrell, C. *Science* **2002**, *297*, 593.
(42) Fagan, J. A.; Simpson, J. R.; Landi, B. J.; Richter, L. J.; Mandelbaum, I.; Bajpai, V.; Ho, D. L.; Raffaelle, R.; Hight Walker, A. R.; Bauer, B. J.; Hobbie, E. K. *Phys. Rev. Lett.* **2007**, *98*, 147402.
(43) Lu, W.; Xiong, Y.; Hassanien, A.; Zhao, W.; Zheng, M.; Chen, L. W. *Nano Lett.* **2009**, *9*, 1668.
(44) Martel, R.; Derycke, V.; Lavoie, C.; Appenzeller, J.; Chan, K. K.; Tersoff, J.; Avouris, Ph. *Phys. Rev. Lett.* **2001**, *87*, 256805.
(45) Haggenmueller, R.; Guthy, C.; Lukes, J. R.; Fischer, J. E.; Winey, K. I. *Macromolecules* **2007**, *40*, 2417.
(46) Matsui, J.; Yamamoto, K.; Miyashita, T. *Carbon* **2009**, *47*, 1444.
(47) Hermant, M. C.; Verhulst, M.; Kyrylyuk, A. V.; Klumperman, B.; Koning, C. E. *Comput. Sci. Technol.* **2009**, *69*, 656.
(48) Hermant, M. C.; Klumperman, B.; Kyrylyuk, A. V.; van der Schoot, P.; Koning, C. E. *Soft Matter* **2009**, *5*, 878.
(49) Any commercial equipment and/or materials identified in this document, or in the published paper to which it refers, are done so in order to adequately specify the experimental conditions and procedures. In no case does such an identification imply any recommendation by NIST or the United States government, nor does it imply that the materials or equipment identified are necessarily the best available for this purpose.

AM9002205